Superalloys 2008
Roger C. Reed, Kenneth A. Green, Pierre Caron, Timothy P. Gabb, Michael G. Fahrmann, Eric S. Huron and Shiela A. Woodard
TMS (The Minerals, Metals & Materials Society), 2008

LONG-TERM CYCLIC OXIDATION BEHAVIOR OF SELECTED HIGH TEMPERATURE ALLOYS

Vinay P. Deodeshmukh and S. Krishna Srivastava
Research and Technology Department, Haynes International Inc., Kokomo, IN 46904-9013
vdeodeshmukh@haynesintl.com and ksrivastava@haynesintl.com

Keywords: long-term cyclic oxidation, Ni- and Fe-based alloys, alumina- and chromia-formers, flowing air, still air

Abstract

Long-term cyclic oxidation resistance is often needed for high temperature alloys used in gas turbine engines for extending their operating lives. This study evaluates the cyclic-oxidation behavior of commercially available Ni- (HAYNES® 230®, 214®, HASTELLOY® X, and HR-160® alloys) and Fe-based alloys (HR-120® and 556® alloys) in flowing air at 982°C, 1093°C, and 1149°C for a total exposure of one year. Test samples were thermally cycled every 30 days at temperature followed by air cooling to room temperature. Alloy performances were assessed by analyzing the weight-change behavior and extent of attack, as measured by metal loss and average internal penetration. The results clearly demonstrated the effects of alloy composition and temperature on long-term cyclic oxidation resistance. The 214 alloy exhibited superior oxidation performance owing to its ability to form and maintain protective alumina scale. Amongst the chromia-formers, 230 alloy performed the best at all temperatures; while Fe-based alloys exhibited rather poor oxidation resistance due to poor scale adhesion. By contrast, the HR-160 alloy showed the lowest weight-loss at 1149°C of the chromia-forming alloys; however, this alloy underwent extensive internal attack. This study also compared cyclic oxidation resistance of 230, HR-120, and HR-160 alloys in flowing and still air. It was found that alloy composition has a profound effect on the extent of oxidation in flowing air compared to that in still air. For instance, the Fe-based HR-120 alloy exhibited improved performance in flowing air while Ni-based alloys (230 and HR-160 alloys) performed better in still air. The factors that may have influenced the oxidation behavior of alloys in flowing and still air will be discussed.

Introduction

The continuous demand for improved performance of high-temperature gas turbine components has led to increasingly severe operating conditions, particularly for advanced systems. Increases in operating temperatures have been achieved in part by modifications in the alloy composition and with the use of internal cooling schemes. However, the useful life of an alloy is frequently limited by its long-term cyclic-oxidation resistance. Wrought Ni- and Fe-based solid-solution strengthened alloys are often used in advanced gas turbines at elevated temperatures for their high temperature strength and environmental resistance. Of particular interest in this study is high temperature cyclic-oxidation, which is an aggressive mode of degradation in gas turbine engine and other high temperature environments.

The performance of high temperature alloys depends critically on the formation of thermally grown oxide (TGO). Ideally, these alloys should form a thermodynamically stable, continuous, slow-growing, and adherent TGO scale [1-3]. It is well known that for long-term protection above 600°C Cr_2O_3, Al_2O_3, and SiO_2 are the principal TGO scales [1-3]. The majority of solid-solution strengthened wrought alloys used in gas turbines rely on the formation of a continuous and exclusive Cr_2O_3 scale for extending the service life. An issue is that long-term use of Ni-Cr and Fe-Cr based alloys at elevated temperature under thermal cycling conditions results in scale spallation due to thermal stresses induced by the mismatch of coefficient of thermal expansion (CTE) between the Cr_2O_3 scale and the underlying alloy substrate [4]. Therefore, advanced high temperature alloys should not only possess excellent spallation resistance, but should also be able to re-establish a protective or semi-protective oxide scale during subsequent oxidation. This requires that the alloys have sufficient chromium content to initially form and then sustain the continued growth of a Cr_2O_3 scale. For this, the alloy needs provide a sufficient Cr diffusion flux towards the alloy/oxide interface. A continuous breakdown and re-growth of Cr_2O_3 scale consequently develops a chromium depleted zone in the subsurface region of the alloy. Furthermore, for greater extent of subsurface chromium depletion it is less likely that the alloy will reform a protective Cr_2O_3 scale. As a consequence, the Cr-depleted surface will be exposed to oxygen which will ultimately lead to the formation of less protective scales. Thus, a more rapid oxidation attack ensues, which in turn severely reduces longevity of gas turbine materials. Gleeson and Harper [5] studied long-term oxidation behavior of various commercial chromia-forming alloys and showed the importance of subsurface characterization of alloy degradation.

Very few solid-solution strengthened wrought alloys form primarily alumina-based scale for prolonged service life. These alloys are typically based on an M-Cr-Al composition in which M represents Ni, Fe, or Ni+Fe. An important criterion in such alloys is that it should have sufficient Al content to establish and maintain external Al_2O_3 scale. This paper compares cyclic-oxidation resistance of chromia- and alumina-forming alloys.

High-temperature alloys are typically used in service conditions for several thousand hours of high temperature exposure under thermal cycling conditions. An extrapolation of short-term (up to 1000h) test data for predicting long-term oxidation behavior could be misleading because breakaway oxidation may occur during service at a time exceeding the duration of short-term testing. Harper *et al.* [6, 7] studied the long-term cyclic oxidation behavior of selected high temperature alloys in still air. It was found that certain alloys exhibit adequate oxidation resistance for several thousands hours, but then eventually undergo rapid breakdown oxidation. These alloys showed extensive scale spallation and formed internal voids and oxides. A further issue is that oxidation testing is frequently carried out in still air and it is possible that vapor species from one alloy may affect the oxidation kinetics of alloys being tested. Moreover, gas turbine components are subjected to gaseous environments flowing at various rates, which may further affect the oxidation kinetics. Therefore, it should be viewed as more relevant to conduct high-temperature oxidation testing in a flowing gas atmosphere for prolonged exposures. It should be noted that thermal cycles of just a few hours are often observed in aero turbines. A thermal cycle period of 30 days

selected in this study relates more towards land-based turbines which involve relatively long cycle period. An increase in cycling frequency results in greater amount of oxide spallation in shorter period thereby significantly reducing component lifetimes.

The wrought forms of Ni- and Fe-based alloys are commonly used for static combustion components in advanced gas-turbine engines. The Ni-based Hastelloy X alloy has been used in the gas turbine industry since 1940's for combustion zone components such as transition ducts, combustor cans, spray bars and flame holders as well as in afterburners, tailpipes and cabin heaters. The more recently developed HAYNES 230, 214, HR-120, HR-160 and 556 alloys were designed for high-temperature strength and/or oxidation resistance. The 230 alloy is a Ni-Cr-W based alloy and is a premier gas turbine alloy currently used in the hot gas components of aero as well as land-based gas turbines. The 214 alloy is Ni-Cr-Al-type alloy, which forms stable Al_2O_3 scale, and hence developed to exhibit excellent oxidation resistance. In the gas-turbine industry it has found application for honeycomb seals, combustor splash plates and other static parts. The HR-160 alloy is based on Ni-Co-Cr-Si system and was developed for service in severe high-temperature corrosion environments. It is widely used in recuperators, heat exchangers, and waste heat recovery systems. The Fe-based HR-120 alloy is based on the Fe-Ni-Cr-Nb system and is strengthened by the addition of nitrogen. It is extensively used for stationary shrouds in a variety of land-based gas turbines. Another Fe-based alloy (556 alloy) was developed for service at elevated temperature in moderately corrosive environments. In gas turbine engines, it has found application in non-rotating components of land-based gas turbines burning low-grade fuels.

The overall objective of this work was two-fold. Firstly, to study the long-term cyclic-oxidation resistance of selected high temperature alloys in flowing air. Secondly, to compare the results obtained in flowing air with that in still air at various temperatures (*i.e.* 982°C, 1093°C, and 1149°C). A part of the long-term cyclic oxidation results in flowing air of selected alloys was recently reported by Srivastava *et al.* [8]; and that in still air by Harper *et al*. [6]. The main thrust of this paper is to more thoroughly characterize and analyze the oxidation performance of the alloys reported by Srivastava *et al.* and to study a few additional high temperature alloys. The alloys selected for cyclic oxidation testing in flowing air were the X, 230, HR-120, HR-160, 214, and 556 alloys. The nominal compositions of these alloys studied are summarized in Table I. Each of these alloys is a chromia-former, except for the 214 alloy.

Experimental Procedures

Wrought alloy samples of approximate dimensions 2.54 cm × 2.54 cm × 1 cm were prepared from mill-annealed plates. The test samples were polished to a 120-grit finish cleaned with acetone and then weighed prior to exposure. The samples with drilled holes were suspended vertically on a rod and placed inside a horizontal alumina-tube furnace. The cyclic oxidation tests were conducted at 982°C, 1093°C, and 1149°C in flowing air for 360 days, *i.e.* 12 cycles of 30 days. The air flow rate used was 55.5 cm^3/s. Cyclic oxidation testing involved thermal cycles at constant testing temperature for a 30-day period followed by air-cooling to room temperature. After the completion of a given 30-day exposure period, the sample boat was removed from the furnace and the samples were allowed to cool to room temperature. Except for the 214 alloy, oxide scale spalled from each sample when cooled to room temperature. No attempt was made to retain any spalled oxide scale during testing or sample handling. Oxidation testing had been carried out in a similar manner in a box furnace to obtain data in still air. The details of the oxidation testing in still air are described by Harper *et al.* [6].

After the completion of 360 days of high-temperature exposure, cross-sections of the oxidized samples were prepared using standard metallographic techniques. The average metal thickness loss was approximated by dividing the final weight loss of the sample by the alloy density. The average internal attack (*i.e.* voids and internal oxide precipitates) in a given sample was measured by optical metallographic examination. Overall, eight measurements were made for each alloy to arrive at an average depth of internal penetration. The average metal affected which includes metal loss from scale formation and spallation plus average internal attack from oxide and void formation was calculated and used for ranking the alloy performances. SEM and EDS analyses were carried out on cross-sections to determine the structure and constitution of the oxide scale and the internal oxide precipitates. The subsurface depletion zone depth was measured using the EDS on selected alloys.

Results and Discussion

Long-term Cyclic Oxidation Resistance in Flowing Air

Figure 1 shows the weight-change behavior of each alloy as a function of time during thermal cycling at 982°C, 1093°C, 1149°C in flowing air. Each alloy except for 214 alloy exhibited weight-loss kinetics after approximately three oxidation cycles. In general, it was found that the amount of weight loss increased considerably with increasing temperature. Table II summarizes the calculated rates of weight change for each of the alloys studied. The linear and parabolic dependencies of alloys are defined using equations 1 and 2.

$$\Delta W = k_l t \quad \ldots\ldots (1)$$

$$\Delta W^2 = k_p t \quad \ldots\ldots (2)$$

where ΔW is weight change as function of time, t and k_l ($mg/cm^2.day$) and k_p ($mg/cm^2.day^{1/2}$) are linear and parabolic rate constants. The weight-loss kinetics were found to be generally linear amongst the chromia-formers. In the case of the 214 alloy it was parabolic and the rate constant increased with increasing temperature. Overall, the rates of weight-loss for the chromia-forming alloys increased by an order of magnitude with increasing temperature from 982 to 1149°C. Two-stage kinetics in which the second stage was greater than the first was observed for most of the chromia-forming alloys at 1093°C and 1149°C. The first-stage rates of weight-loss are for the initial rather protective oxide scale; while the second-stage rates correspond to the non-protective scale formed after breakdown of the more protective Cr_2O_3-rich scale. It is interesting to note that scale breakdown on the Fe-containing HR-120 and X alloys at 1093°C occurred earlier (after just 5 cycles) compared to Ni-based 230 and HR-160 alloys (after 8 cycles). While at 1149°C protective-scale breakdown occurred just after a few thermal cycles (< 5 cycles) for all chromia-forming alloys. In addition, the rates of weight-loss during the second stage at 1149°C were orders of magnitude greater than the second-stage rates measured at 1093°C. It is clearly evident from the weight-change behavior that the Fe-containing X, HR-120, and 556 alloys showed extremely high

weight-loss at T ≥ 1093°C, reflecting rather poor oxidation resistance.

The best performing alloy at all temperatures by far was 214 alloy, which exhibited minor weight-gain after all oxidation exposures. Based solely on the weight-change kinetics, 230 alloy was the best-performing alloy amongst the chromia-formers at 982°C and 1093°C, while it was HR-160 alloy at 1149°C; however, it should be noted that rankings based on the weight-change kinetics are subject to change when total metal affected is considered. Indeed, for a structural component the *total* amount of metal affected by oxidation is of extreme importance because of its load-bearing function. The total metal affected includes metal loss from scale formation and spallation plus internal attack from oxide and void formation. Metallographic measurements in the form of metal loss and average internal penetration were conducted using optical microscopy. It is seen in Fig. 2 that the 214 alloy showed very little or no internal penetration, confirming that it had the best oxidation resistance amongst the alloys tested. Amongst chromia-formers when total degradation is considered, the 230 alloy exhibited the best oxidation resistance at all temperatures. These measurements gave a similar ranking that was observed from the weight-change kinetics except for the ranking of HR-160 alloy, particularly at 1149°C. When total degradation is considered, it is seen in Fig. 2 that HR-160 alloy underwent higher oxidation attack than the 230 and HR-120 alloys at all temperatures. This is because HR-160 alloy underwent greater internal penetration compared to other chromia-formers. The present results clearly show the importance of assessing subsurface degradation in conjunction with weight-change measurements.

To further evaluate the amount of oxidation attack from internal penetration, the fraction of internal attack (f_{ip}) was calculated from metal loss and average internal penetration as follows,

$$f_{ip} = \frac{\text{Average internal penetration}}{\text{Average internal penetration + metal loss}}$$

The fraction of internal attack (f_{ip}) due to the internal penetration along with the results of metal loss and average internal penetration are tabulated in Table III. It is seen that internal oxidation penetration attack was the principal mode of attack for all the alloys at 982°C, with f_{ip} values greater than 0.85. The f_{ip} values decreased considerably with increasing temperatures such that principal mode of degradation at 1149°C becomes metal loss. In particular, f_{ip} values at 1149°C were found to be less than 0.25 for all the alloys except HR-160, which had a value of 0.74. As indicated in Fig. 3, there is a marked difference in the way HR-160 oxidizes compared to the other chromia-forming alloys studied. This figure clearly shows that the extent of internal penetration in a representative chromia-forming 230 alloy was less at 982°C and the extent of internal attack remained similar even at 1149°C. By contrast, in the case HR-160 alloy internal oxide penetration and void formation increased considerably from 982°C to 1149°C. It is also interesting to note that the mode of attack transformed from internal attack to metal loss (*i.e.* lower f_{ip} values) with temperature increase from 982°C to 1093°C for alloys which contain significant amount of Fe (*i.e.* HR-120, X and 556 alloys). This suggests that these alloys form less protective oxides even at 1093°C and exhibit rather poor scale adhesion at higher temperatures. In summary, based on the weight-change kinetics and extent of attack, the overall ranking to long-term cyclic-oxidation resistance in flowing air from best to worst is as follows:

214 >> 230 > HR-120 > HR-160 > X > 556.

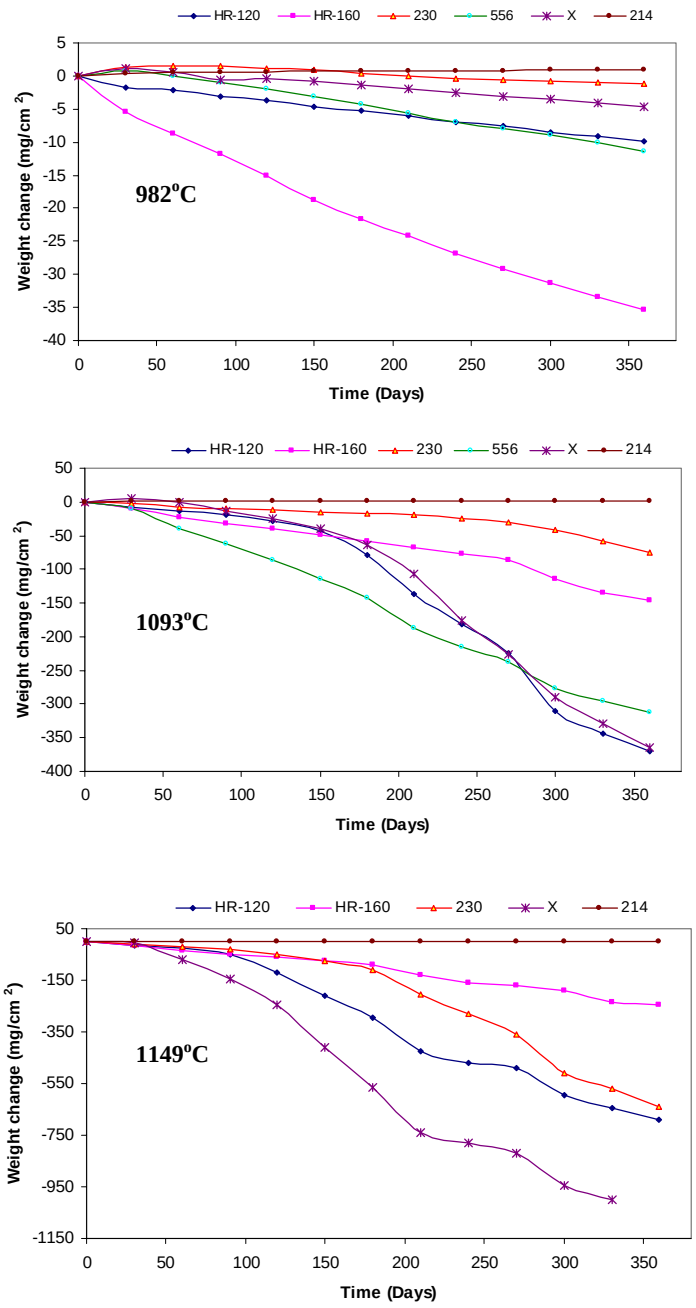

Fig. 1. Weight-change vs time plots for the cyclic oxidation of selected alloys in flowing air at 942, 1093, 1149°C.

Table I. Nominal Compositions (wt%) of the alloys studied.

Alloy	Ni	Fe	Cr	Co	Mo	W	C	Others
X	47[a]	18	22	1.5	9	0.6	0.1	1Mn*, 1Si*, 0.5Al, 0.008B*
230	57[a]	3	22	5	3	14	0.1	0.5Mn, 0.4Si, 0.3Al, 0.02La, 0.015B*
214	75	3	16	2*	0.5*	0.5*	0.04	4.5Al, 0.1Zr, 0.01Y, 0.01B*
HR-120	37	33[a]	25	3*	1*	0.5*	0.05	0.7Mn, 0.7Nb, 0.2N, 0.6Si, 0.1Al, 0.04B
HR-160	37	2*	28	29	1*	1*	0.05	2.75Si, 0.5Mn, 0.4Al*, 0.5Ti
556	20	31[a]	22	18	3*	2.5	0.1	1Mn, 0.6Si, 0.6Ta, 0.2N, 0.02Zr

[a]As balance; *Maximum

Table II. Rates of weight change for the alloys tested under cyclic conditions in flowing air at 982°C, 1093°C, and 1149°C.

Alloy	k_l at 982°C (mg/cm^2 day)	k_l at 1093°C (mg/cm^2 day)	k_l at 1149°C (mg/cm^2 day)
214	+0.003* (2-11)	+0.005* (2-10)	+0.008* (2-6)[3]
230	+0.023* (1-2) -0.008 (3-12)	-0.097 (1-8) -0.427 (9-12)	-0.542 (1-5) -3.04 (6-12)
HR-160	-0.096 (1-12)	-0.312 (1-8) -0.652 (9-12)	-0.499 (1-2) -0.776 (3-12)
HR-120	-0.026 (2-12)	-0.238 (1-4) -1.663 (5-12)	-0.637 (1-3) -2.418 (3-12)
X	-0.015 (1-12)	-0.388 (1-5) -1.735 (6-12)	-2.29 (1-3) -5.032 (3-7)
556	-0.035 (2-12)	-0.936 (1-12)	NA

Notes: 1. Numbers in parentheses represent the cycle numbers.
2. *Parabolic rate constant, k_p (mg/cm^2 day$^{1/2}$).
3. Sample suffered weight-loss after 6 cycles.

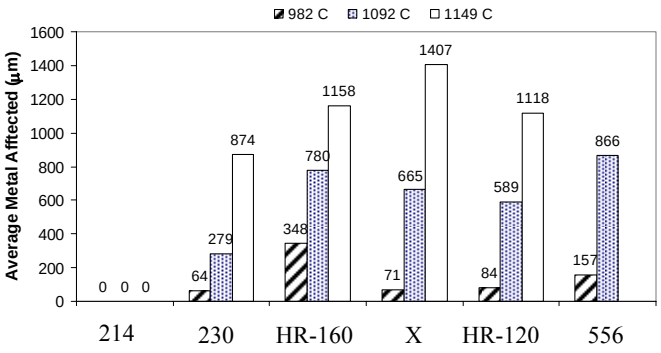

Fig. 2. Average Metal Affected (metal loss + average internal penetration) of alloys tested in flowing air at 942, 1093, 1149°C.

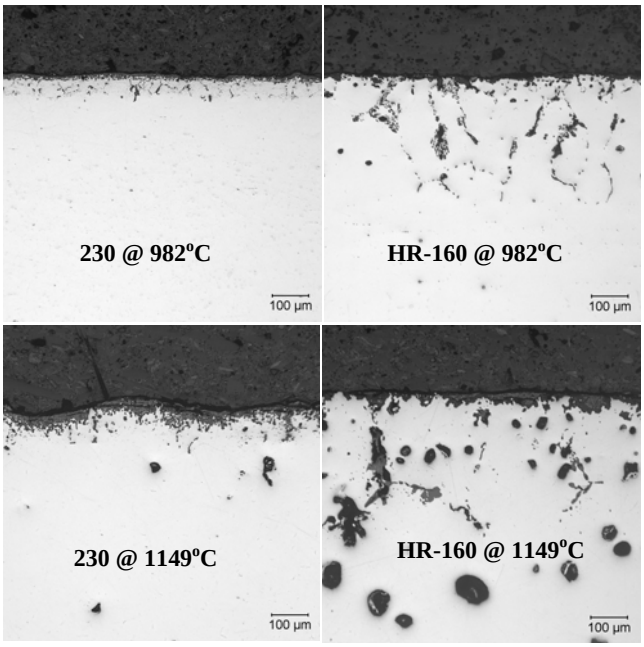

Fig. 3. Optical micrographs of 230 and HR-160 alloys tested in flowing air at 982°C and 1149°C.

Cross-sectional SEM images of the alloys after long-term oxidation testing in flowing air at 1149°C are shown in Fig. 4. It is seen that very little external oxide scale remained on the alloys except for the 214 alloy. In addition, internal precipitates and void formation are clearly evident in most of the chromia-forming alloys. EDS analysis was carried out on the oxidized samples to characterize the internal oxide precipitates and remaining external oxide scales. The 214 alloy formed a planar, slow-growing, and adherent external Al_2O_3 scale. The formation of such a protective scale conferred excellent oxidation resistance. The 214 alloy is a Ni-Cr-Al type alloy which is able to establish a continuous Al_2O_3 scale even with just 4.5 wt% Al. It is well known that a lower amount Al content is needed to establish and maintain an Al_2O_3 scale on M-Cr-Al alloys (where M is Ni, Fe or Ni+Fe) than on the M-Al alloys [1-3]. In addition, the presence of reactive elements such as Zr (0.1wt %) and Y (0.01wt %) in the 214 alloy resulted in the formation of slow-growing and adherent Al_2O_3 scale. Pint *et al.* found that a combination of two or more reactive elements in Al_2O_3-forming alloys significantly improves oxide scale adhesion compared to a single reactive element addition [9].

Table III. Metal loss, average internal penetration, and fraction of internal attack (f_{ip}) for the alloys tested in flowing air at 982°C, 1093°C, and 1149°C

Alloy	982°C			1093°C			1149°C		
	Metal loss (μm)	Av. Int. Pen. (μm)	f_{ip}	Metal loss (μm)	Av. Int. Pen. (μm)	f_{ip}	Metal loss (μm)	Av. Int. Pen. (μm)	f_{ip}
214	0	0	0	0	0	0	0	0	0
230	3	61	0.96	86	193	0.69	724	150	0.17
HR-160	43	305	0.88	180	599	0.77	305	853	0.74
HR-120	13	71	0.85	460	130	0.22	853	264	0.24
X	5	66	0.93	434	231	0.35	1308	99	0.07
556	13	145	0.92	381	485	0.56	NA	NA	NA

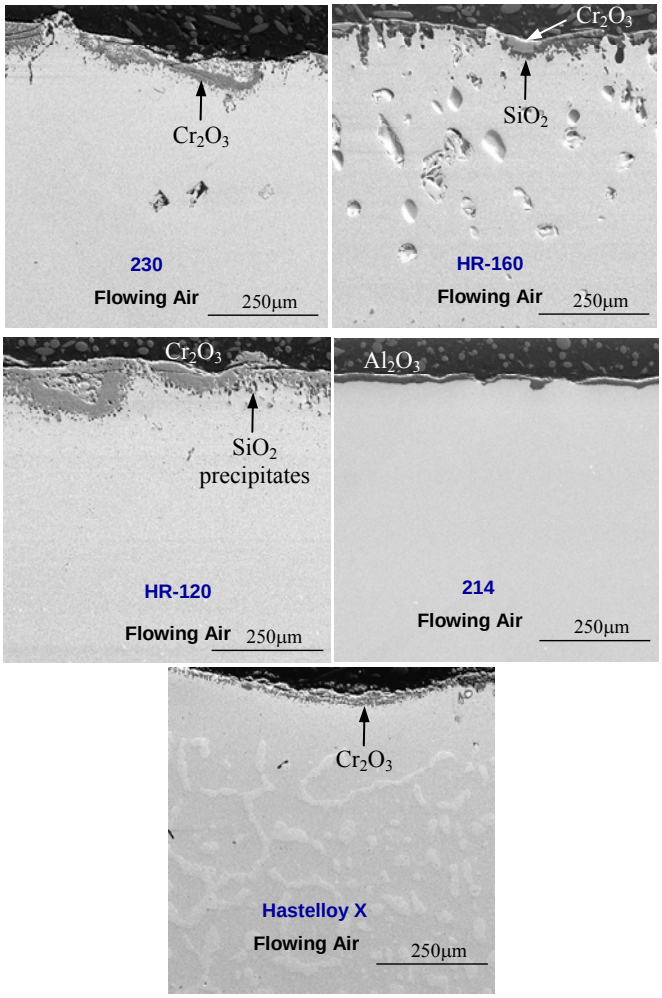

Fig. 4. Cross-sectional SEM images of alloys tested for 360 days in flowing air at 1149°C.

The chromia-forming alloys underwent extensive scale spallation and showed internal oxidation at 1149°C (Fig. 4). In general, an external Cr-rich oxide scale was detected and several scale cracks were observed within the scale in almost all the chromia-forming alloys. There was hardly any scale left on the 230 alloy but at few locations a very thin oxide scale was found, which apparently consisted of a relatively thin outer layer of $MnCr_2O_4$ spinel followed by inner Cr_2O_3 scale. X-ray diffraction performed on the oxidized 230 alloy also indicated formation of $NiWO_4$ and NiO. Cr-rich and Al-rich internal oxide precipitates and voids were also detected in the 230 alloy. The improved oxidation performance of 230 alloy amongst the chromia-formers is attributable to the formation of $MnCr_2O_4$ spinel and the presence of a reactive element (0.02 wt% La) addition [5-8]. Specifically, and as will be discussed in more detail in Section 3.2, is believed that the formation of an outermost $MnCr_2O_4$ spinel layer reduces Cr_2O_3 volatilization and addition of La improves scale adhesion, thereby improving its oxidation resistance at higher temperatures. The SEM and EDS analyses indicated that surface scales on the X and HR-120 alloys were neither adherent nor continuous. Both alloys showed presence of Cr-rich, Ni-rich, and Fe-rich oxides within the scale, which are believed to be Cr_2O_3, NiO, and Fe_2O_3 respectively. A rapid oxidation attack of the Fe-based alloys at higher temperatures is attributable to early breakdown of Cr_2O_3 scale and subsequent formation of fast-growing and less-protective Fe_2O_3 and NiO oxides. The internal Si-rich and Al-rich oxide precipitates, inferred to be SiO_2 and Al_2O_3, were also detected in the HR-120 alloy. In accordance with the measurements of average internal penetration it is seen that HR-160 formed deep internal precipitates and voids throughout the cross-section (Fig. 4). The HR-160 formed a Si-rich oxide-scale layer beneath the external Cr-rich oxide scale. The former was inferred to be SiO_2. Addition of Si is known to improve the oxidation resistance of chromia-forming alloys [10-12]; however, it is also known to decrease scale spallation resistance [12-14]. Apparently, the nominally 2.75 wt% Si addition in the HR-160 alloy forms a continuous SiO_2 layer at the chromia/alloy interface and this in turn may have considerably decreased scale adhesion particularly at 982°C. It is seen from Table III that HR-160 alloy underwent considerable metal loss (~ 43 μm) at 982°C even though it contains sufficient amount of Cr to establish a protective oxide scale. This is atleast partly attributable to the poor scale adhesion of HR-160 alloy due to Si addition.

The weight change and metallographic measurements of metal affected are very useful in differentiating accelerated oxidation attack; however, it does not always reflect the total amount of alloy affected by the oxidation process. Thus, additional characterization of the subsurface and interfacial elemental concentration is necessary. The subsurface concentration profiles and interfacial elemental contents of Cr in particular, for

the 230, HR-120, HR-160, and 214 alloys, were analyzed using EDS. The EDS spectra were calibrated before each run with an alloy standard and depletion or enrichment of a given element is considered to be fairly accurate. Figure 5 presents subsurface concentration profiles in 230, HR-120, HR-160, and 214 alloys after a total of 360 days oxidation at 1149°C. The profile depth and interfacial Cr content appear to differ significantly between the alloys, i.e.,

HR-160 alloy: ~1600 μm and 8 wt%
230 alloy: ~600 μm and 4.6 wt%,
HR-120 alloys: ~500 μm and 4.8 wt%
214 alloy: ~ 50 μm and 2.5wt% Al/16.7wt% Cr

It was found that Cr depletion extended the most into the HR-160 alloy compared to 230 and HR-120 alloys. The comparatively shallow Cr depletion in HR-120 and 230 alloys is clearly a consequence of the large metal loss incurred by these alloys at 1149°C (Table III). It is seen that there is hardly any Cr depletion and only a minor Al-depleted region in the 214 alloy. The HR-160 alloy showed the highest interfacial Cr content compared to 230 and HR-120 alloys. Indeed, Li and Gleeson [12] showed the beneficial effect of Si addition (2.75 wt%) in improving the interfacial Cr content in Ni-Cr-Co alloy system. However, it should be noted that 8 wt% is still insufficient to establish a continuous Cr_2O_3 scale on a bare alloy, and once initial breakdown occurs in HR-160 alloy, it becomes susceptible to a rapid internal oxidation because of its relatively high Si content. In conjunction with the Cr depletion, each of the alloys showed Ni enrichment near the alloy/oxide interface. The Ni enrichment in the alloy was on the order of approximately 17wt% for HR-120 alloy, 10wt% for HR-160 alloy, 15wt% for 230 alloy, and 2 wt% for 214 alloy.

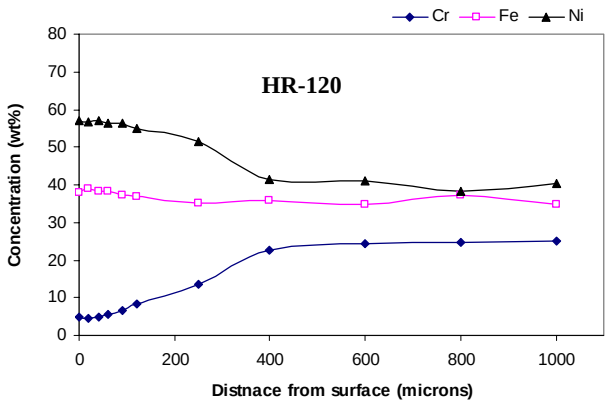

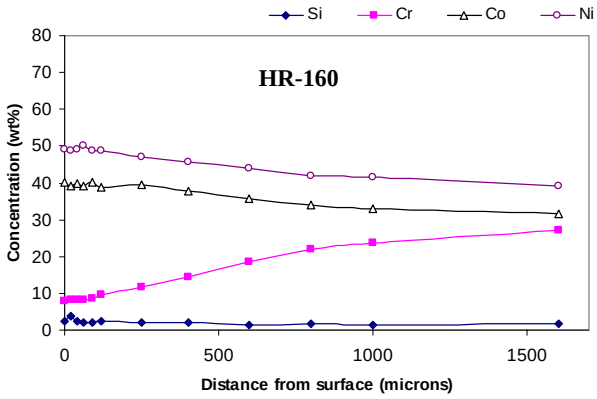

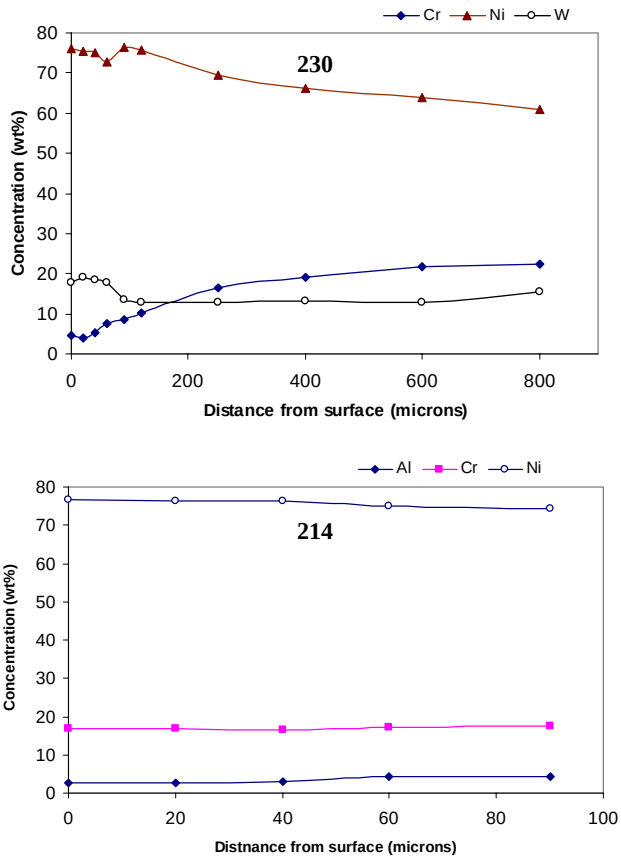

Fig. 5. Concentration profiles of HR-120, HR-160, 230, and 214 alloys tested in flowing air at 1149°C.

The HR-160 alloy showed a Co enrichment of 10wt%; while, 230 showed an enrichment of W (6 wt%) and HR-120 exhibited enrichment of Fe (3 wt%). The alumina-forming 214 alloy, showed a depletion of Al (1.7 wt%) at the alloy/oxide interface.

Comparative Cyclic Oxidation Resistance of Selected Alloys in Flowing and Still Air

The weight-change kinetics of three selected alloys (*i.e.* HR-120, HR-160 and 230) in flowing air at 982°C, 1093°C, 1149°C are compared in Fig. 6 with the kinetics obtained in still air. The ranking of the alloys based on the weight-change kinetics was quite similar for the two types of testing, with 230 alloy being the best-performing alloy at 982°C, and 1093°C; while HR-160 alloy is apparently the best-performing alloy at 1149°C. The extent of weight-loss was significantly different in each testing method. The weight-loss kinetics were faster (*i.e.* greater weight loss) when 230 and HR-160 alloys were exposed to flowing air; while it was slower in the case of HR-120 alloy for all temperatures. The difference in the weight-loss kinetics was found to increase with increase in temperature, and it was quite significant particularly for the 230 alloy at 1149°C. As shown in the previous section, weight-change behavior may be a misleading metric when ranking the alloy performances. Therefore, a comparison of weight-loss kinetics as well as total subsurface degradation is necessary and the results are summarized in Table IV. The average metal affected and fraction of internal attack was not available in the case of still air

at 982°C because experiments were carried out for a longer exposure period (*i.e.* for 2 years). It is seen that the order of performance under both the conditions is still the same, with 230 being the best followed by HR-120 and HR-160 alloys. However, in addition to greater weight-loss it is also seen that the average metal affected is higher in the case of 230 and HR-160 alloys in flowing air, except for the HR-160 alloy at 1149°C.

To further evaluate and quantify the amount of alloy composition affected by each testing method, f_{ip} values must be compared (Table IV). For instance, even though HR-160 alloy showed greater average metal affected in still air at 1149°C, a comparison of the f_{ip} values clearly show that internal attack is a more dominant mode of degradation in still air (f_{ip} =0.87) than in flowing air (f_{ip}=0.74). The f_{ip} value was also greater in still air than in flowing air for the 230 and HR-160 alloys at 1093°C and 1149°C. In fact, in the case of 230 alloy the principal mode of degradation at 1149°C was metal loss in flowing air (f_{ip} = 0.17), while it was internal attack in still air (f_{ip} = 0.67). This contrast in the mode of attack was clearly evident from SEM images of 230 alloy after the exposures to flowing and still air (Fig. 7). It is seen that the 230 alloy underwent rather extensive internal oxide and void formation in still air while internal penetration was comparatively smaller in flowing air. Also, the external scale was still visible after exposure to still air, while there was hardly any scale left for the case of flowing air. The trend in HR-120 alloy is reversed with the average metal affected being lower in flowing air than in still air. As expected, when f_{ip} values for HR-120 alloy are compared, it is found that metal loss was a less dominant mode of degradation (*i.e.* less metal loss) in flowing air (*e.g.* f_{ip} = 0.22 at 1093°C) than in still air (*e.g.* f_{ip} = 0.14 at 1093°C). The results presented so far clearly prove that alloys perform quite differently in flowing air and still air. It also shows the manner in which environmental conditions (flowing air or still air) and alloy composition often influence the oxidation performance of alloys.

The factors that may have influenced the oxidation behavior in flowing and still air will now be briefly discussed. The change in extent of attack is at least partly attributable to the different vaporization rates of Cr_2O_3 scale in flowing and still air. The Cr_2O_3 vaporization thermodynamics and kinetics for reaction (A) below were reviewed in detail by Rapp [15] and are considered for the current experimental testing conditions.

$$\frac{1}{2}Cr_2O_3 + \frac{3}{4}O_2(g) \rightarrow CrO_3(g) \qquad \ldots\ldots \qquad (A)$$

The maximum possible rate of vaporization ($G^{\max}_{CrO_3}$) in gravimetric units can be calculated using the Hertz-Langmuir equation:

$$G^{\max}_{CrO_3}\left(\frac{g}{cm^2.s}\right) = \frac{\alpha P_{CrO_3}}{2.256\times10^{-2}}\left(\frac{M_{CrO_3}}{T}\right)^{1/2} \qquad \ldots\ldots \qquad (3)$$

Rapp showed that the rate of metal recession per side, R, may be calculated by further multiplying equation 3 by the specific volume of Cr in the alloy (~0.127cm^3/g).

$$R_{alloy}(mils/h) = (5.7\times10^7)\frac{P_{CrO_3}}{T^{1/2}} \qquad \ldots\ldots \qquad (4)$$

In the above equations $MCrO_3$ is the molecular weight of CrO_3, α is the evaporation coefficient which is fraction of maximum possible rate (*i.e.* ≈1) for a given conditions, and $PCrO_3$ can be calculated analytically in accordance with the following equation,

$$\log P_{CrO_3} = \frac{-12{,}250}{T} + 3.04 + \frac{3}{4}\log P_{O_2} \ldots\ldots (5)$$

Using the above equations, the equilibrium vapor pressure of CrO_3 (g) and the maximum possible Cr weight loss for the present conditions can be plotted as a function of temperature (Fig. 8).

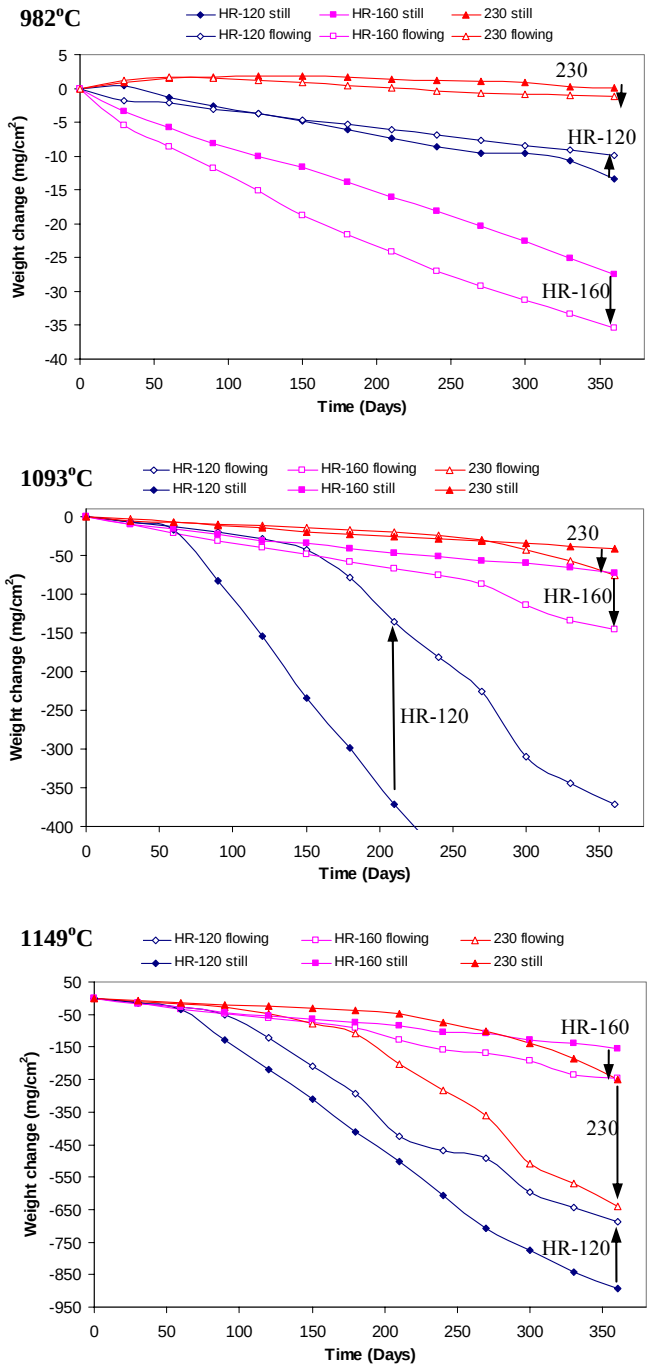

Fig. 6. Comparative weight-change vs. time plots for cyclic oxidation in flowing air and still air for 230, HR-160, and HR-120 alloys at 982°C, 1093°C and 1149°C.

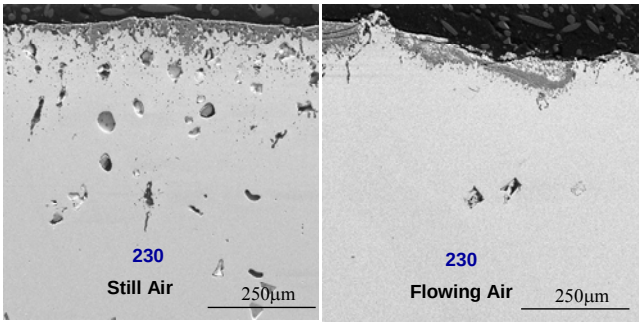

Fig. 7. Comparison of cross-sectional SEM images of 230 alloy tested in flowing air and still air at 1149°C for 360 days.

It is seen that the equilibrium vapor pressure of CrO_3 (g) and maximum possible Cr weight loss considerably increases with increasing temperature. In fact, it is found that the maximum possible Cr weight loss is significantly greater than the observed total weight loss for alloys during oxidation testing. For example, at 1150°C the maximum Cr weight loss and metal recession due to Cr_2O_3 vaporization is 151 g/cm^2.y and 26.4 x 10^4 μm/y, which is much larger than the total weight loss and metal recession per side observed for each alloy after oxidation testing at 1149°C (Figs. 1 and 2). Thus, it is possible to lose more CrO_3 (g) in flowing air than in still air by sweeping away the reaction product. Indeed, it was reported by Graham and Davis [16] and Asteman *et al.* [17] that increasing the flowing gas velocity caused an increase in the vaporization rates of Cr_2O_3. According to Rapp [15], the net vaporization rate of Cr_2O_3 will approach the maximum predicted by the Hertz-Langmuir approximation (Eq. (1) and Fig. 8) in turbulent gases at near sonic speed. Moreover, a continuous flow of air during the flowing-air test provides a constant supply of moisture on to the test samples. The presence of moisture considerably accelerates Cr_2O_3 vaporization rates, particularly at higher temperatures [15, 16, and 18] and may have further accelerated oxidation kinetics of chromia-forming alloys.

It was observed that the internal attack was the less dominant mode of degradation for 230 and HR-160 alloys in flowing air while for HR-120 alloy metal loss was the less dominant mode of degradation in still air. The 230 and HR-160 alloys form a Cr-rich outer scale and it is believed that the difference in weight-loss between flowing and still air is at least partly attributable to an increase in Cr_2O_3 vaporization rate in flowing air. By contrast, HR-120 alloy contains 33wt% Fe which results in the formation of a non-protective Fe-rich oxide scale over time. In fact, Gleeson and Harper also suggested that HR-120 alloy forms Fe-rich oxide scale in still air during extended exposure [5]. It is postulated that the formation of Fe-rich oxides on HR-120 alloy after initial scale spallation may have prevented the rapid vaporization Cr_2O_3 scale seen in 230 and HR-160 alloys. The other factors that can affect the oxidation kinetics are different heating rates due to different sample dimensions, spallation resistance, and formation of vapor species of Mo and W. The samples used in the present flowing air study were thinner than the ones used in still air testing by 0.64 cm. The thinner samples used in flowing air resulted in a faster heating rate compared to samples used in still air. The formation of vapor species of Mo and W may have been possible from the 230, X, 556, and HR-120 alloys, which contain those elements. However, the formation of such volatile species is expected to be less likely to affect oxidation kinetics in flowing air. Indeed, Peters *et al.* reported that oxidation of Ni-Cr-Mo alloys was severely affected in still atmosphere compared to flowing atmosphere [19]. It is believed that the volatilization of Cr_2O_3 is not a major factor in determining the difference in oxidation behavior of HR-120 alloy in flowing and still air; however, volatile species of Mo and W are most likely to affect its oxidation behavior in still air. The results presented in this paper clearly emphasize the importance of high temperature oxidation testing in flowing gas atmosphere for prolonged exposure.

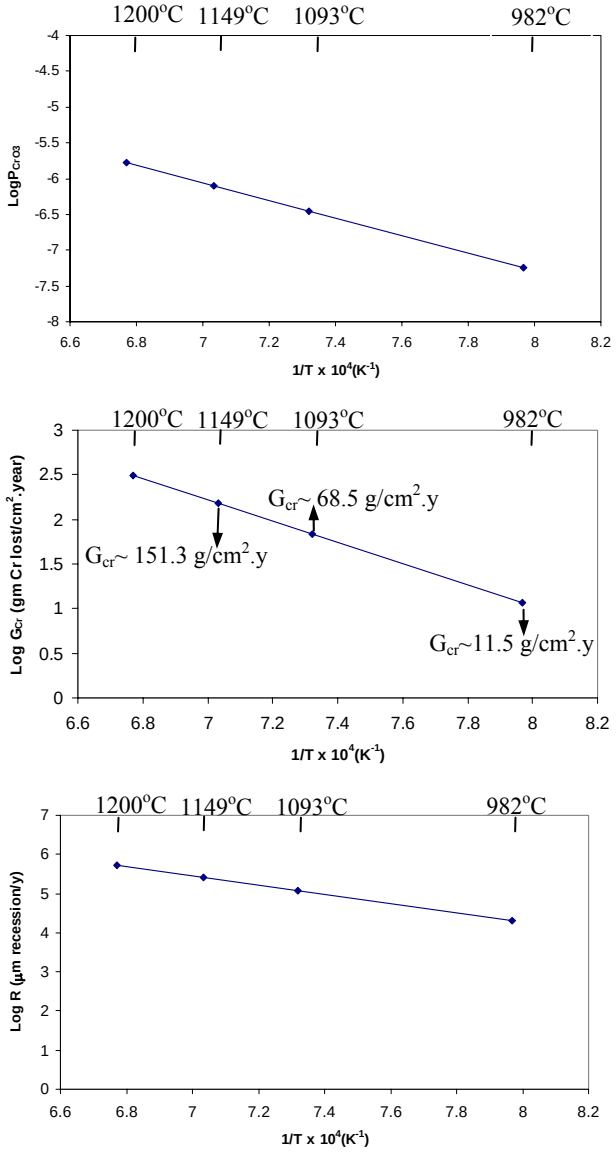

Fig.8. Equilibrium vapor pressure of CrO_3 (g), maximum vaporization rates of Cr_2O_3 and rate of metal recession per side between 982-1200°C.

Table IV. Comparison of weight-loss, average metal affected, and fraction of internal attack (f_{ip}) in flowing air and still air for the 230, HR-120, and HR-160 alloys exposed at 982°C, 1093°C, and 1149°C for 360 days.

Alloy	982°C		1093°C						1149°C					
	Weight-loss (mg/cm^2)		Weight-loss (mg/cm^2)		Av. Metal Aff. (μm)		f_{ip}		Weight-loss (mg/cm^2)		Av. Metal Aff. (μm)		f_{ip}	
	flowing air	Still air	flowing air	Still air	flowing air	Still air	flowing air	Still air	flowing air	Still air	flowing air	Still air	flowing air	Still air
230	-1.2	0.05	-75.4	-42.1	279	272	0.69	0.82	-639.1	-249.7	874	864	0.17	0.67
HR-120	-9.9	-13.4	-370.8	-665.7	589	965	0.22	0.14	-688.1	-894.2	1118	1346	0.24	0.18
HR-160	-35.4	-27.4	-145.8	-73.1	780	737	0.77	0.88	-246.2	-155.5	1158	1491	0.74	0.87

Summary and Conclusions

The 214 alloy outperformed all the chromia-forming alloys from the standpoint of long-term cyclic oxidation resistance in flowing air. The improved performance of 214 alloy was attributed to the formation of protective and adherent Al_2O_3 scale. The best performing of the chromia-formers was 230 alloy at all temperatures, while Fe-containing X and 556 alloys exhibited poor oxidation resistance due to poor scale adhesion thus eventually resulting in the formation of less-protective Fe-rich oxides. The formation of $MnCr_2O_4$ above Cr_2O_3 scale and the presence of 0.02% La were beneficial in improving oxidation resistance of 230 alloy. An additional Fe-based HR-120 alloy performed relatively better; however, it also underwent extensive scale spallation after long-term exposure at 1093°C and 1149°C and formed Fe-rich oxides. The subsurface degradation analysis showed that a dominant mode of attack was internal oxide penetration particularly at lower temperatures of 982°C and 1093°C, while it transformed into metal loss at 1149°C for all alloys except for the HR-160 alloy which exhibited rather poor oxidation resistance when subsurface degradation was considered. It is believed that formation of SiO_2 scale beneath the Cr_2O_3 scale was helpful in decreasing oxidation kinetics; however, apparently it also decreased the scale adhesion particularly at 982°C.

The cyclic oxidation behavior of alloys in still air and flowing air is quite different and their performance in these environments depends upon the alloy composition and testing temperature. It was found that Fe-based alloy HR-120 exhibited improved performance in flowing air and Ni-based alloys (230 and HR-160) performed better in still air. The higher degree of metal loss for 230 and HR-160 alloys in flowing air is at least partly attributable to larger Cr_2O_3 vaporization. The other factors that may have influenced the oxidation kinetics in still and flowing air at various temperatures are different heating rates, spallation resistance, and formation of vapor species of Mo and W. Overall, the results presented in this paper clearly demonstrate that environmental (*i.e.* flowing or still air) conditions and alloy compositional factors often influence the oxidation performance of Ni-Cr and Fe-Cr based alloys.

Acknowledgements

We would like to thank M.J. Newburn, J.P. Cotner, and M.A. Richeson for their assistance and expertise in oxidation experiments, electron and optical microscopy and late J.E. Barnes for his many contributions. Discussions on this subject particularly on the vaporization rates of chromia with Prof. Brian Gleeson at University of Pittsburgh have been highly beneficial and are much appreciated.

References

1. J. Smialek and G.H. Meier, "High Temperature Oxidation", *Superalloys II,* ed. C.T. Sims, N.S. Stoloff, and W.C. Hagel (New York, NY: John Wiley & Sons, Inc., 1987), 293-326.

2. P. Kofstad, *High Temperature Corrosion*, (Elsevier Applied Science, 1988), 342-421.

3. N. Birks, G.H. Meier, and F.S. Pettit, *Introduction to the High Temperature Oxidation of Metals*, 2nd Edition, (Cambridge University Press, 2006), 115-127.

4. M. Schütze, "Mechanical Properties of Oxide Scales", *Oxidation of Metals*, 44, (1995), 29-61.

5. B. Gleeson and M.A. Harper, "The long-Term, Cyclic-Oxidation Behavior of Selected Chromia-Forming Alloys" *Oxidation of Metals*, 49, (1998), 373-399.

6. M.A. Harper, J.E. Barnes, and G.Y. Lai, "Long-Term Oxidation Behavior of Selected High Temperature Alloys", *CORROSION/97*, National Association of Corrosion Engineers, Paper#97132, Houston, TX, (1997).

7. M.A. Harper and B. Gleeson, "Long-Term, Cyclic Oxidation Behavior of Three Chromia-Forming Alloys Exposed to Air at 982°C" *Cyclic Oxidation of High Temperature Materials*, Proceedings of EFC Workshop, ed. M. Schütze and W.J. Quadakkers, Frankfurt/Main, (IOM Communications,1999), 273-286.

8. S.K. Srivastava, M.J. Newburn, J.P. Cotner, and M.A. Richeson, "Long-Term Oxidation Behavior of Selected High Temperature Alloys", *ASME Turbo Expo 2007*, American Society of Mechanical Engineers, Paper#GT2007-28269, Montreal, Canada, (2007).

9. B.A. Pint, K.L. More, and I.G. Wright, "The Use of Two Reactive Elements to Optimize Oxidation Performance of Alumina-Forming Alloys", *Materials At High Temperatures*, 20(3), (2003), 375-386.

10. D.L. Douglass and J.S. Armijo, "The Effect of Si and Mn on the Oxidation Mechanism of Ni-20Cr", *Oxidation of Metals,* 2, (1970), 207-231.

11. A. Kumar and D.L. Douglass, "Modification of the Oxidation Behavior of High-purity Austenitic Fe-14Cr-14Ni by the Addition of Si", *Oxidation of Metals,* 10, (1976), 1-22.

12. B. Li and B. Gleeson, "Effects of Silicon on the Oxidation Behavior of Ni-base Chromia-forming Alloys", *Oxidation of Metals,* 65, (2006), 101-122.

13. E. Evans, D.A. Hilton, R.A. Holm, and S.J. Webster, "Influence of Si Additions on the Oxidation Resistance of a Stainless Steel", *Oxidation of Metals,* 19, (1983), 1-18.

14. F.H. Stott, G.J. Gabriel, F.I. Wei, and G.C. Wood, "The Development of Silicon-containing Oxides during the Oxidation of Iron-Chromium-Base Alloys" *Werkstoff Und Korrosion*, 38, (1987), 521-531.

15. R.A. Rapp, "Vaporization Losses from Cr_2O_3 Protective Scales", *AGARD High Temperature Corrosion of Aerospace Alloys*, International Organization, (1973), 147-154.

16. H.C. Graham and H.H. Davis, "Oxidation/Vaporization Kinetics of Cr_2O_3", *Journal of American Ceramic Society,* 54, (1971), 89-93.

17. E. Asteman, J.E. Svensson, L.G. Johansson, "Evidence of Chromium Evaporation Influencing the Oxidation of 304L: The Effect of Temperature and Flow Rate", *Oxidation of Metals*, 57, (2002), 193-216.

18. B.A. Pint and D.J. Young, "Chromium Volatilization Rates from Cr_2O_3 Scales into Flowing Gases Containing Water Vapor", *Oxidation of Metals*, 66, (2006), 137-153.

19. K.R. Peters, D.P. Whittle, and J. Stringer, "Oxidation and Hot Corrosion of Ni-Based Alloys Containing Molybdenum", *Corrosion Science*, 16, (1976), 791-804.